

Deep Neural Network-Based Voltage Prediction for Alkali-Metal-Ion Battery Materials

Sk Mujaffar Hossain,[†] Namitha Anna Koshi,[†] Seung-Cheol Lee,^{*,†,‡} G.P Das,^{*,¶}
and Satadeep Bhattacharjee^{*,†}

[†]*Indo-Korea Science and Technology Center (IKST), Bangalore 560064, India*

[‡]*Electronic Materials Research Center, Korea Institute of Science & Technology, Korea*

[¶]*Research Institute for Sustainable Energy (RISE), TCG-CREST, Kolkata 700091, India*

E-mail: leesc@kist.re.kr; gour.das@tcgcrest.org; s.bhattacharjee@ikst.res.in

Abstract

Accurately predicting the voltage of battery materials is essential for advancing energy storage technologies and designing more efficient, high-performance batteries. In this study, we developed a deep neural network (DNN) model to predict the average voltage of materials used in Li-ion, Na-ion, and other alkali-metal-ion batteries. A comprehensive dataset was compiled from the Materials Project, incorporating a diverse set of features, including structural, physical, chemical, electronic, and thermodynamic properties, along with battery-specific descriptors. These features were utilized to construct a robust DNN model aimed at facilitating the discovery of novel battery materials. The model performance evaluated through 10-fold cross validation achieving an R^2 value of 0.99 and a mean absolute error (MAE) of 0.069 V on the validation dataset. This high level of accuracy underscores the model's capability to capture the complex relationship between material properties and electrochemical performance. Furthermore, the results demonstrate that machine learning approaches,

particularly DNN models, can provide rapid and reliable voltage predictions without relying on computationally expensive first-principles calculations. This research shows how systematic data analysis can accelerate the identification and improvement of next-generation battery materials. By focusing on key material properties and using computational methods, our study lays the groundwork for faster development of new energy storage solutions.

Introduction

In different disciplines of science and technology, the rational design of modern materials is the ultimate goal. Over the past one to two decades, tremendous effort has been made by the materials science community to compile the large dataset of materials with different properties from multiple sources¹⁻³ so as to provide easy access of database repository to scientists and engineers to aid in novel materials discovery using artificial intelligence (AI) and machine learning (ML). In every domain such as material science, medical science, social science, advance technology, etc., there is a growing demand for new high performance, highly efficient and robust materials. To meet this demand, researchers have intensified their efforts in various fields of material science, such as high temperature superconductivity,⁴⁻⁶ solar cell,⁷⁻¹⁰ energy storage and beyond.

Since last couple of decades, the Li-ion battery (LIB) is being used as a prominent renewable energy storage device and is reigning in all major electronic applications from tiny watch to large battery in EV sector and it captures most of the shares in the commercial market.¹¹ But different environment friendly renewable energy sources (solar, wind, etc.) and their utilization augments the need for higher density and highly durable energy storage materials. High manufacturing cost, low abundance of Li metal and paucity of other constituent metallic elements used in the electrode and other factors hinder further commercialization of existing battery technology to meet the current demand.¹¹ To overcome these challenges, researchers are moving towards anode-free metal-ion battery^{12,13} and other earth abundant

active metal-ion battery such as Na, Zn etc.¹⁴⁻¹⁷

Developing new electrode materials with high energy density and long cycle life, comparable to lithium-ion batteries (LIBs), remains a significant challenge. The process is not only technically demanding but also costly and time-consuming due to the complexities of laboratory synthesis and experimental validation. To solve these issues, researchers are trying to utilize the fast growing and high-in demand AI¹⁸ and ML¹⁹ techniques with the latest updated battery data repository such as Materials Project (MP),²⁰ OQMD,^{21,22} AFlowLib,²³ ESP,²⁴ CMR,²⁵ NOMAD,²⁶ ICSD,²⁷ COD,²⁸ NASA,^{29,30} etc.

Significant progress has recently been experienced in the search of new electrode materials, via prediction of battery voltages,^{31,32} volume change,³² chemical reaction,³³ and formation energy³³ of electrode materials using a variety of ML techniques in conjunction with the well captured clean battery database. This database^{2,3} has been predominantly created using the quantum mechanical density functional theory (DFT) calculations. By combining the DFT structured database with improved and sophisticated ML algorithms, one can accelerate the discovery of modern electrode materials. Various regression and classification-based ML models have been employed for both the design and prediction of new electrode materials. For instance, Joshi et al. utilized deep neural networks (DNNs), support vector regression (SVR), and kernel ridge regression (KRR) to predict electrode voltages for metal-ion batteries, achieving a mean absolute error (MAE) of approximately 0.43 V after 10-fold cross-validation.³¹ Similarly, Moses et al. developed a regression-based DNN model to predict the volume change of electrode materials during charge and discharge cycles, reporting an MAE of 0.47 V for average voltage predictions.³² Moreover, Louis et al. employed Graph Neural Networks (GNNs) to predict battery voltages using two different strategies, chemical reaction energy and formation energy-based approaches, obtaining MAE values in the range of 0.31 to 0.34 V.³³

Beyond voltage prediction, ML-driven research has also expanded towards the rational design of high-energy-density cathode and anode materials, where models are trained to screen

novel compositions with optimized electrochemical stability and fast ion diffusion kinetics.³⁴ Additionally, ML techniques are being leveraged for the discovery of solid-state electrolytes (SSEs), aiming to enhance ionic conductivity while maintaining chemical and electrochemical stability.³⁴⁻³⁶ Liquid electrolytes have also been explored using ML approaches,³⁷ particularly in predicting solvation energy,³⁸⁻⁴⁰ electrochemical window,^{41,42} and ionic mobility,^{35,43} which are crucial for improving battery safety and performance.^{7,37} Another important avenue is battery health diagnostics and lifetime prediction,⁴⁴⁻⁴⁶ where ML-based models analyze degradation mechanisms, capacity fade trends, and structural stability over prolonged cycling.

As AI and ML techniques continue to evolve with larger datasets, improved feature selection strategies, and more sophisticated deep-learning architectures, their role in battery materials discovery and optimization will only grow stronger. The combination of DFT-driven data generation and ML-guided material screening has already proven to be a powerful synergy, paving the way for the next generation of high-performance, durable, and sustainable energy storage materials.⁴⁷

The development of high energy-density Li-ion and Na-ion battery materials has gained significant attention in both academia and industry. However, complex phase transitions during insertion and extraction, lead to challenges such as poor cycle stability, low energy density, and limited rate capability. To address these challenges, researchers have explored various strategies for optimizing Li/Na-ion cathodes. In this work, we leverage a DNN model developed using the PyTorch library to design novel layered transition metal oxide based compositions. Our model is robust and highly predictive, outperforming previously published approaches for voltage prediction.³¹⁻³³

Feature engineering plays a crucial role in materials informatics, where properties derived from chemical, structural, elemental, electronic, and thermodynamic representations are used to construct feature vectors. By incorporating these effective strategies, we trained our DNN model to predict the voltage of electrode materials with high accuracy. As a result,

we identified several promising cathode materials for Na-ion batteries with high voltage and energy density. To validate our predictions, we further conducted first-principles DFT simulations, confirming the potential of these materials for next-generation Na-ion batteries.

Methods

Collection of Data Set and their Distribution

In this work, we have collected all the metal-ion battery data from the open access Materials Project (MP, v2022.10.28) database using the Pymatgen Material Genomes tools (pymatgen).^{20,48} We have extracted 4351 data for all the metal-ion batteries with DFT computed voltage and their corresponding battery features with structure. The number distribution of 10 different alkali metal-ion batteries is shown in Figure 1(a) in a bar plot and their corresponding weight percentage (pie plot) in the domain of metal-ion battery is given in Figure 1(b). It clearly shows that Li-metal ion battery dominates the dataset when compared to other metal-ion batteries. Also, we plot the average voltage distribution of the dataset (shown in Figure 1(c)), with the values ranging from 0 to 6.5 V and it signifies the number of available data distribution with certain voltage.

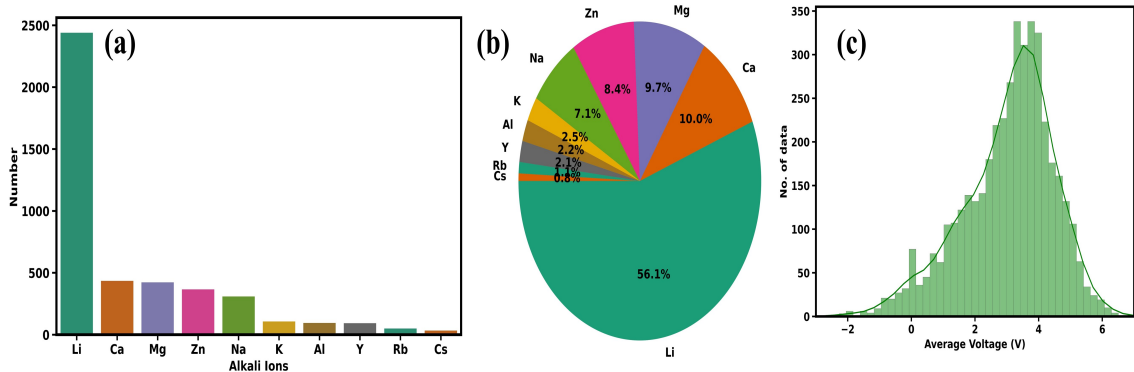


Figure 1: Statistical distribution of (a) 10 different alkali working metal-ion battery (b) % population of metal-ion in the battery data set and (c) Average voltage distribution.

Model Architecture and Features Generation

The features of each charge and discharge electrode of all battery materials in the MP dataset were constructed using different composition based feature generation tools such as Matminer⁴⁹ and Xenonpy.^{50,51} Along with key battery-related features, we also incorporate the statistical elemental properties of all constituent elements in each electrode composition. This approach helps capture the unique fingerprint of each electrode material within the dataset, enhancing the model’s ability to differentiate and predict material properties accurately. The statistical elemental feature will be different for a specific electrode material, and by considering all the statistical variables (like avg, min, max, and var) we have generated almost 262 features (see Figure 2) and used them as input for DNN model. Out of 262 features, we have generated 232 features from Xenonpy and other are extracted from Matminer and battery explorer of MP. The components of a feature vector are diverse in terms of their magnitudes, which can range from small fractions to a few thousands. Therefore, all the input features were normalized for better and more efficient training of the DNN model thereby avoiding any biased preference of a particular feature with respect to others based solely on their magnitude. The normalization was performed by effectively scaling all of the inputs to be between -1 and 1, and it was carried out on the fly while training our model and it is not done for target value. The list of statical features used to develop the DNN model is provided in the Table S1 of the Supporting Information (SI).

Model Details

To predict the average voltage of any electrode material (cathode or anode) we implemented a DNN based on the battery electrode material properties. The architecture of the DNN was designed and implemented using PyTorch,^{52,53} a flexible deep learning framework. The model consisted of the following layers: input layer, hidden layers, dropout layers, and output layer. The input layer accepts a feature vector derived from material properties, where the feature size corresponds to the preprocessed dataset dimensions. The network included 5 hidden

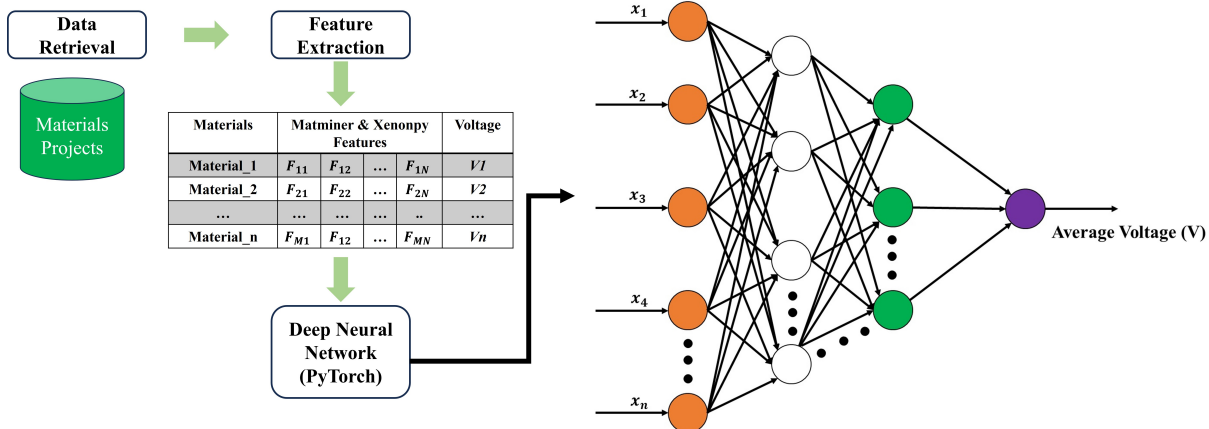


Figure 2: Workflow and DNN model architecture.

fully connected layers, each with 262 neurons. Nonlinear activation functions, specifically LeakyReLU (Leaky Rectified Linear Unit), were applied to introduce nonlinearity and also prevent overfitting. Dropout regularization was incorporated with a dropout probability of 0.2 to prevent overfitting and improve generalization by randomly dropping neurons during training. The output layer consisted of a single neuron with a linear activation function, providing the predicted value of average voltage. The Mean Squared Error (MSE) loss was used to quantify the prediction errors. MSE was chosen for its sensitivity to large errors, ensuring the model minimizes significant deviations in voltage predictions. The Adam optimizer⁵⁴ was utilized for its efficiency and adaptive learning rate capabilities. The learning rate and weight decay was set to 0.0001 and 0.001.

For training, the dataset was split into training and testing subsets, with 80% of the data allocated for training and the remainder for testing. The model was trained over 1000 epochs with a batch size of 64, balancing computational efficiency and convergence. A learning rate scheduler with StepLR was employed to dynamically adjust the learning rate, ensuring better convergence. During training, both training and validation losses were monitored to ensure the model’s performance improved without overfitting. A residual plot showed that the prediction errors were well-distributed around zero, with no significant bias observed. The network architecture was defined using PyTorch’s `torch.nn.Module`. The model param-

eters were updated iteratively using backpropagation, and gradients were computed using PyTorch’s autograd functionality. After each epoch, the model was evaluated on the validation set to monitor generalization performance. The DNN demonstrated R^2 value of 0.995 and 0.906 for training and testing with MSE value of 0.009 and 0.182 indicating its effectiveness in predicting the average voltage of battery materials. The model’s predictions closely matched the actual values (Figure 4), highlighting its ability to learn complex relationships between input features and the target variable.

Results and discussion

The performance of the ML models has been tested through different error metrics, mean absolute error (MAE) and mean square error (MSE). The MAE and MSE are defined by the following equations

$$MAE = \frac{1}{N} \sum_{i=1}^N (|V_i^{DFT} - V_i^{ML}|) \tag{1}$$

$$MSE = \frac{1}{N} \sum_{i=1}^N (V_i^{DFT} - V_i^{ML})^2 \tag{2}$$

where V_i^{DFT} represents the DFT computed voltage and V_i^{ML} represents the machine learning predicted voltage, for the given i^{th} battery sample and N total number of samples in the dataset.

The loss during the training of the model was evaluated as shown in Figure 3(a). At the beginning of training (epochs close to 0), both training and testing losses are high, which is expected because the model starts with randomly initialized weights. It has not yet learned to map the input features to the target output effectively. In the first few epochs, both the training and testing losses drop steeply. This indicates that the model is learning rapidly and adjusting its weights effectively to minimize the error. As training progresses, the loss

values for both training and testing data begin to plateau. This suggests that the model has learnt the underlying patterns in the data and is approaching convergence. The training loss and testing loss closely follow each other throughout the training process. This is a strong indicator that the model is generalizing well to unseen data and is not overfitting. At the final epochs (e.g., around 1000), both training and testing losses remain low and stable, further confirming that the model has achieved a good fit without overfitting or underfitting. The convergence of training and training losses demonstrates the model’s capability to learn and generalize effectively. The lack of significant divergence between the two curves suggests that the chosen hyperparameters (learning rate, architecture, etc.) are appropriate. The alignment of the testing loss with the training loss highlights that the model is not overly complex and has a good balance of bias and variance.

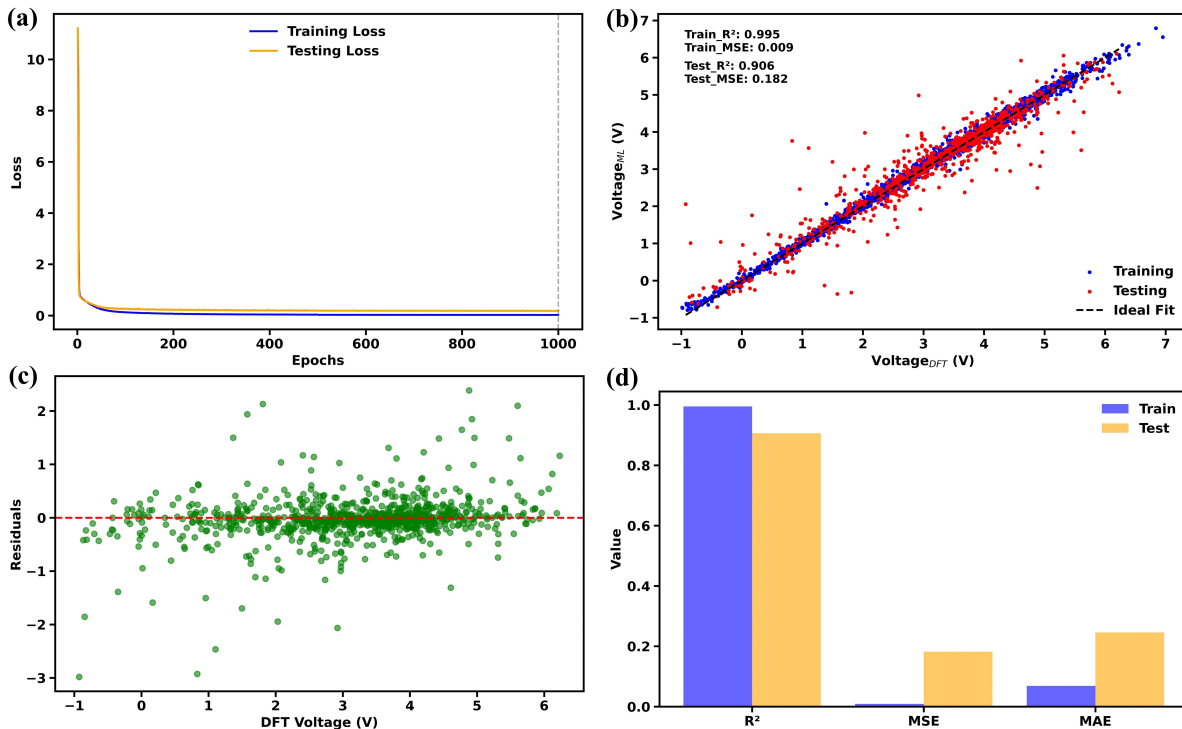


Figure 3: Training and testing of DNN model (a) loss with epochs, (b) DFT voltage and ML predicted voltage, (c) residuals of actual and predicted voltage, and (d) metric value.

The R^2 and MSE value of training and testing presented in Figure 3(b), shows a near-perfect R^2 and very low MSE for training set indicates that the model has successfully learned

the patterns in the training data. The test R^2 value of 0.906 shows that the model captures most of the variance in the test data. Some scatter points deviate significantly from the ideal fit line, especially at higher actual voltage values. These deviations indicate instances where the model struggle to predict accurately. The higher MSE on the test set (0.182 vs. 0.009, Figure 3(d) reflects that very small prediction errors could be present on unseen data, which is common in machine learning models. The model demonstrates strong learning on the training set and reasonable generalization on the test set, as evidenced by the high test R^2 and close alignment of many points with the ideal fit line ($y = x$). Minor overfitting may exist, but the model can still make accurate predictions for the majority of the test data. From the MSE and MAE values (0.182 and 0.24V respectively), it can be concluded that our DNN model shows excellent performance as compared to the earlier reported ML models, with the respective MAE³¹⁻³³ shown in Table 1. The error bar plot in Figure 3(d) compares the mean error metrics of our model. It shows a smaller MAE with respect to the previously reported MAE values by Joshi et al.³¹ and Moses et al.³²

The residuals appear fairly symmetric around the zero line (Figure 3(c)), which suggests that the model does not have significant bias toward overestimating or underestimating the actual values. Most residuals are clustered close to the zero line, indicating that the model’s predictions are generally accurate.

Table 1: Comparison of our DNN model and other models

Models	R^2	MAE	Source
DNNs	0.81	0.43	Joshi et al. ³¹
DNNs	0.83	0.39	Moses et al. ³²
GNNs	- - -	0.34	Louis et al. ³³
DNNs	0.91	0.24	Present work

Validation of the model

Model validation is crucial for testing its excellent performance verification and evaluation. We validate our DNN model by considering experimentally observed and commercially avail-

able battery electrode material for both Li and Na-ion battery (see Table 2). We obtained a R^2 and MSE values of 0.991 and 0.012V respectively, as presented in Figure 4 which suggests the excellency of our model.

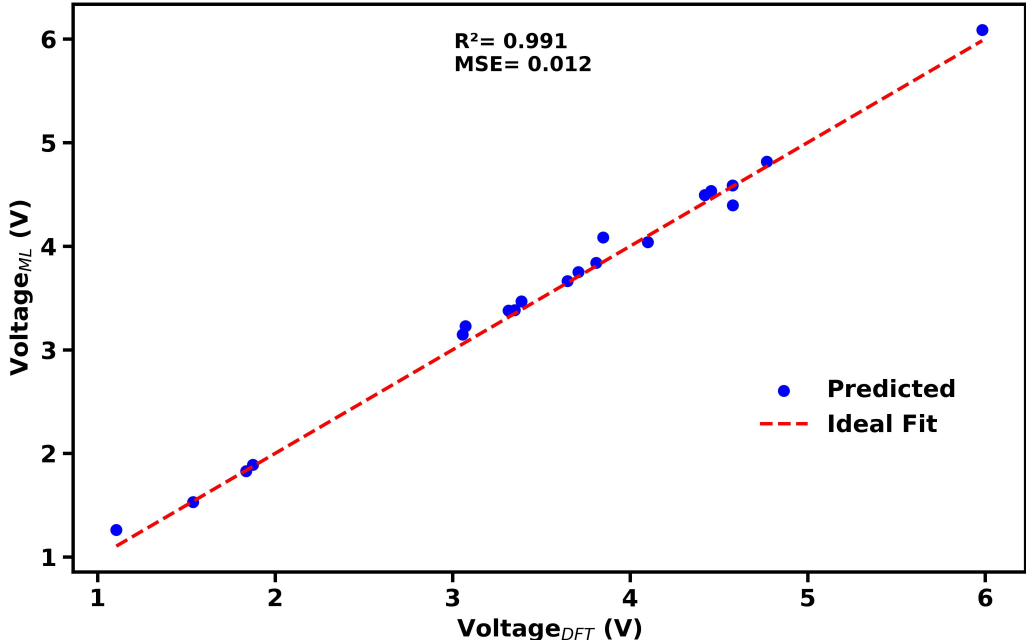


Figure 4: Model validation with DFT data of experimentally available electrode materials.

The list of materials used for the validation are shown in Table 2 along with voltage data obtained from DFT, our DNN model, and experiment. The absolute deviation of our model predicted voltage with experimental and DFT voltages are evaluated through the following expressions: $\Delta V_1 = |V_{DFT} - V_{DNN}|$ and $\Delta V_2 = |V_{expt.} - V_{DNN}|$ respectively, and tabulated in Table 2.

Our model is developed based on DFT data of battery materials and its associated features, ensuring that the deviation (ΔV_1) between our DNN model’s predicted voltage and the DFT-calculated voltage remains minimal for nearly all validation materials. In contrast, a larger deviation (ΔV_2) is observed when comparing the predicted values to experimental data. This discrepancy is expected, as the voltage of battery materials is influenced by various experimental conditions such as humidity, temperature, and pressure—factors that are not accounted for in the DFT dataset. Despite these challenges, our model demonstrates

Table 2: DNN predicted vs experimental and DFT voltages and their deviation

Materials	$V_{expt.}$	V_{DFT}	V_{DNN}	ΔV_1	ΔV_2
LiCoO ₂	4.1 ⁵⁵	3.808	3.803	0.005	0.297
LiFePO ₄	3.5 ⁵⁶	3.847	3.845	0.002	0.345
LiMnPO ₄	4.1 ⁵⁷	4.578	4.207	0.371	0.107
LiCoPO ₄	4.8 ⁵⁸	4.770	4.753	0.017	0.047
LiNiO ₂	3.85 ⁵⁶	4.099	4.079	0.020	0.229
LiMn ₂ O ₄	4.15 ⁵⁹	4.577	4.545	0.032	0.395
LiTiS ₂	2.1 ⁶⁰	1.875	1.866	0.009	0.234
LiNiPO ₄	5.3 ⁶¹	5.983	5.957	0.026	0.657
Li ₃ V ₂ (PO ₄) ₃	3.8 ⁶²	3.708	3.716	0.008	0.084
Na ₃ V ₂ (PO ₄) ₃	3.4 ⁶²	3.349	3.361	0.012	0.039
NaCoO ₂	2.8 ^{63,64}	3.056	3.043	0.013	0.243
NaNiO ₂	3.0 ⁶⁵	3.315	3.277	0.038	0.277
NaTiO ₂	1.5 ⁶⁶	1.106	1.104	0.002	0.396
NaFePO ₄	3.0 ⁶⁷	3.072	3.046	0.026	0.046

the ability to predict experimental voltages with minimal error, as evidenced by several cases presented in Table 2.

The Rise of Na-Ion Batteries in Energy Storage

Researchers are increasingly focusing on sodium-ion (Na-ion) batteries as a promising alternative to lithium-ion (Li-ion) technology due to several key advantages in cost, resource availability, and sustainability. One of the most significant benefits of Na-ion batteries is their lower material cost, with a theoretical cost of \$40-77/kWh, making them 30% cheaper than LiFePO₄ based lithium-ion batteries.^{68,69} This cost advantage is particularly crucial given the rising costs and scarcity of lithium, which has led to an increase in production expenses for Li-ion batteries, reaching an average of \$137/kWh in 2020. In terms of energy density, Na-ion batteries offer up to 290 Wh/kg for active materials and 250-375 Wh/L volumetric energy density, making them competitive for energy storage applications. However, current practical Na-ion prototypes have a lower energy density (75-200 Wh/kg) compared to lithium-ion equivalents, but continuous research and development are expected to improve these values.

Another critical factor driving Na-ion battery research is cycle life. While early prototypes have shown faster degradation, some advanced Na-ion battery designs have demonstrated 4,000 cycles, rivaling lithium-ion batteries.^{68,70} This long cycle life is particularly attractive for applications such as grid storage, where energy density is less critical than longevity and cost-effectiveness. Overall, the growing interest in Na-ion batteries stems from their potential to provide a sustainable, cost-effective, and scalable energy storage solution without the resource limitations associated with lithium. As research progresses, improvements in energy density, stability, and charge-discharge performance could make Na-ion batteries a viable alternative to Li-ion batteries for a wide range of applications, including renewable energy storage, electric vehicles, and large-scale power grids. As a result the development of Na-ion battery materials has gained significant attention in both academia and industry.

Among various Na-ion cathode materials, many industries (such as HiNa, CATL, Faradian, Tiamat, etc) has focused on layered transition metal oxides of O3 and P2-types as it emerged as highly promising due to their superior capacity compared to poly-anionic and Prussian blue-based cathodes.⁷¹ However, the large ionic size of Na^+ slows down the kinetics and induces complex phase transitions during insertion and extraction, leading to challenges such as poor cycle stability, low energy density, and limited rate capability. To address these challenges, researchers have explored various strategies for optimizing Na-ion cathodes. In this work, we leverage a DNN model developed using the PyTorch library to design novel O3- and P2-type layered transition metal oxide compositions.

Design Novel Cathode for Na-ion Batteries

The design of new Na-ion battery cathode materials was carried out by leveraging the template crystal structures of transition metal layered oxides with the general formula NaMO_2 , where M represents transition or post-transition metals. These layered oxides serve as a fundamental structural framework due to their well-established electrochemical properties and stability in Na-ion battery applications. For this study, we focused on two widely stud-

ied structural types of layered transition metal oxides: O3-type and P2-type materials (see Figure 5). The O3-type materials exhibit trigonal symmetry with the $R-3m$ space group, while the P2-type materials possess hexagonal symmetry with the $P6_3/mmc$ space group. These two structural configurations were carefully considered in designing new compositions due to their distinct sodium diffusion pathways and electrochemical characteristics.

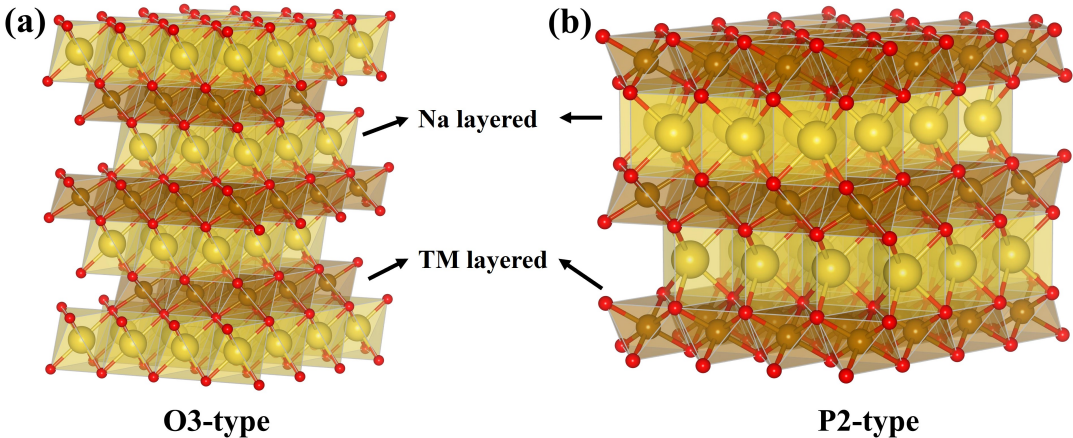


Figure 5: Structure of transition metal layered oxide of (a) O3 and (b) P2-type.

To generate novel compositions, we explored a wide range of 3d transition metals (Cr, Ti, V, Mn, Fe, Ni, Co, Cu, Zn) along with other selected metal species (Al, Mg, Sr), aiming to achieve an optimal balance of critical electrochemical properties. The primary selection criteria for these elements were: phase stability, high voltage, long cycle life, efficient Na-ion diffusion, and fast charging capability. The Supercell package⁷² was utilized to systematically explore and enumerate various element combinations within the NaMO_2 framework. This computational approach enabled the creation of an extensive library of potential compositions by generating numerous atomic substitutions within the host structure. The resulting dataset includes a large number of unique chemical compositions for both O3- and P2-type cathodes, each exhibiting distinct electrochemical and structural properties.

First Principles Calculation

All density functional theory (DFT) calculations were performed using the Vienna Ab initio Simulation Package (VASP)^{73,74} with spin-polarized ferromagnetic ordering. The formation energy calculations employed the generalized gradient approximation (GGA) with the Perdew–Burke–Ernzerhof (PBE) exchange–correlation functional.⁷⁵ For voltage calculations, we applied the Hubbard correction parameters (U) to account for self-interaction errors, and the DFT-D3 method⁷⁶ was used to incorporate dispersion effects for all compounds of interest. The U parameters used for Fe, Mn, Ni, Co, Cr, and Cu were 3.9, 4.0, 6.2, 3.32, 3.7, and 5.5 eV, respectively, as obtained from Ref.^{77,78} A kinetic energy cutoff of 500 eV and a Γ -centered k-point mesh of $11 \times 7 \times 3$ for O3 and $3 \times 3 \times 2$ for P2-type materials was found to be sufficient for achieving convergence. During structural optimization, atomic positions were allowed to relax until the Hellmann–Feynman forces were reduced below 0.01 eV/Å. The electronic minimization was performed with a convergence criterion of 10^{-6} eV. The new composition of charge balance structure for both O3 and P2-type was build using Supercell package.⁷² To generate the new compositions, here we have consider $2 \times 3 \times 1$ supercell lattice for O3-type and $3 \times 3 \times 1$ supercell lattice for P2-type materials.

The formation energy per formula unit (eV/f.u.) has been calculated using the below formula:^{79,80}

$$E_f = E(Na_x M_1^a M_2^b M_3^c O_2) - x\mu_{Na} - a\mu_{M_1} - b\mu_{M_2} - c\mu_{M_3} - \mu_{O_2} \quad (3)$$

Where $a + b + c = 1$ and M_1^a , M_2^b and M_3^c , represents the three different stoichiometry of metallic cations and their corresponding chemical potentials μ_{M_1} , μ_{M_2} , and μ_{M_3} repectively. Again μ_{Na} and μ_{O_2} represents the chemical potential of Na bulk and O_2 molecule.

The voltage (V) of the newly designed compositions was calculated using the general formula⁸¹ for multi-component layered metal oxide which is

$$V = -\frac{E_{Na_{x_2}MO_2} - E_{Na_{x_1}MO_2} - (x_2 - x_1)E_{Na}}{x_2 - x_1} \quad (4)$$

Where M is the multi-cations of different stoichiometry of M_1^a , M_2^b and M_3^c ; E_{Na} is total energy of the Na bulk and x_1 and x_2 are the different sodium (Na) concentration during sodiation and desodiation.

A comprehensive list of the newly designed O3 and P2-type cathode materials, along with their predicted voltages (V) from our DNN model, is presented in Figure 6. The voltage predictions were obtained using our PyTorch-based DNN model, which has demonstrated superior accuracy in predicting the electrochemical performance of Na-ion cathodes. To further validate the stability and feasibility of these newly designed compositions, we performed first-principles DFT calculations. Table 3 and 4 represent the formation energy newly design material compositions, assessing their thermodynamic stability and likelihood of successful synthesis. A detailed discussion of the DFT results, including computed formation energies and structural analyses, is provided in the Supporting Information (SI) section.

Table 3: New composition of O3-type materials for Na-ion battery

O3-type Compositions	Formation energy (eV/f.u.)
$\text{NaMn}_{0.61}\text{Ni}_{0.28}\text{Cr}_{0.11}\text{O}_2$	-7.31
$\text{Na}_{0.67}\text{Mn}_{0.61}\text{Ni}_{0.28}\text{Cr}_{0.11}\text{O}_2$	-6.69
$\text{Na}_{0.33}\text{Mn}_{0.61}\text{Ni}_{0.28}\text{Cr}_{0.11}\text{O}_2$	-5.70
$\text{Na}_{0.83}\text{Mn}_{0.5}\text{Fe}_{0.28}\text{Cu}_{0.11}\text{Mg}_{0.11}\text{O}_2$	-7.12
$\text{Na}_{0.94}\text{Mn}_{0.5}\text{Fe}_{0.28}\text{Cu}_{0.11}\text{Mg}_{0.11}\text{O}_2$	-7.33
$\text{Na}_{0.67}\text{Mn}_{0.5}\text{Ni}_{0.28}\text{Ti}_{0.11}\text{Cr}_{0.11}\text{O}_2$	-7.03
$\text{NaMn}_{0.5}\text{Fe}_{0.33}\text{Cu}_{0.06}\text{Mg}_{0.11}\text{O}_2$	-7.47
$\text{NaMn}_{0.5}\text{Fe}_{0.28}\text{Al}_{0.11}\text{Mg}_{0.11}\text{O}_2$	-7.99
$\text{NaMn}_{0.5}\text{Fe}_{0.28}\text{Cu}_{0.11}\text{Al}_{0.11}\text{O}_2$	-7.48
$\text{NaMn}_{0.5}\text{Fe}_{0.28}\text{Cu}_{0.11}\text{Cr}_{0.11}\text{O}_2$	-7.11

Model Predicted vs DFT Calculated Voltage

Using DFT calculations within the GGA+U framework, we have validated the voltage predictions generated by our DNN model for specific compositions: O3- $\text{Na}_{0.67}\text{Mn}_{0.61}\text{Ni}_{0.28}\text{Cr}_{0.11}\text{O}_2$

Table 4: New composition of P2-type materials for Na-ion battery

P2-type Compositions	Formation energy (eV/f.u.)
$\text{NaMn}_{0.5}\text{Fe}_{0.28}\text{Cu}_{0.22}\text{O}_2$	-6.42
$\text{Na}_{0.89}\text{Mn}_{0.5}\text{Fe}_{0.28}\text{Cu}_{0.22}\text{O}_2$	-6.58
$\text{Na}_{0.83}\text{Mn}_{0.5}\text{Fe}_{0.28}\text{Cu}_{0.22}\text{O}_2$	-6.66
$\text{Na}_{0.72}\text{Mn}_{0.5}\text{Fe}_{0.28}\text{Cu}_{0.22}\text{O}_2$	-6.82
$\text{Na}_{0.67}\text{Mn}_{0.5}\text{Fe}_{0.28}\text{Cu}_{0.22}\text{O}_2$	-6.89
$\text{Na}_{0.67}\text{Mn}_{0.5}\text{Fe}_{0.33}\text{Zn}_{0.17}\text{O}_2$	-7.09
$\text{Na}_{0.67}\text{Mn}_{0.5}\text{Fe}_{0.33}\text{Mg}_{0.17}\text{O}_2$	-7.06
$\text{Na}_{0.67}\text{Mn}_{0.5}\text{Fe}_{0.33}\text{Sr}_{0.17}\text{O}_2$	-7.06
$\text{Na}_{0.67}\text{Mn}_{0.5}\text{Fe}_{0.33}\text{Ba}_{0.17}\text{O}_2$	-7.02
$\text{Na}_{0.67}\text{Mn}_{0.5}\text{Fe}_{0.28}\text{Ni}_{0.22}\text{O}_2$	-6.63
$\text{Na}_{0.67}\text{Mn}_{0.5}\text{Fe}_{0.28}\text{Co}_{0.17}\text{O}_2$	-6.20
$\text{Na}_{0.67}\text{Mn}_{0.5}\text{Fe}_{0.28}\text{Ti}_{0.22}\text{O}_2$	-5.99
$\text{Na}_{0.67}\text{Mn}_{0.5}\text{Fe}_{0.28}\text{Al}_{0.22}\text{O}_2$	-6.97

and P2- $\text{Na}_{0.67}\text{Mn}_{0.5}\text{Fe}_{0.28}\text{Cu}_{0.22}\text{O}_2$. These compositions, highlighted in red in Figure 6(a, b), were selected as representative validation points to avoid the computational expense of performing DFT calculations for all possible compositions. The DNN-predicted voltages for O3- $\text{Na}_{0.67}\text{Mn}_{0.61}\text{Ni}_{0.28}\text{Cr}_{0.11}\text{O}_2$ and P2- $\text{Na}_{0.67}\text{Mn}_{0.5}\text{Fe}_{0.28}\text{Cu}_{0.22}\text{O}_2$ are 3.79 and 3.76V, respectively, while the corresponding DFT-calculated voltages are 3.84 and 3.68V (see SI), as shown in Figure 6(a, b). The minimal errors of just 1.3% and 2.2% demonstrate an excellent agreement between the two methods. This strong correlation highlights the robustness and reliability of our machine learning model in accurately predicting voltages while significantly reducing the computational cost associated with traditional first-principles calculations. The consistency between DFT and DNN results underscore the potential of our model as a powerful tool for screening and predicting the electrochemical properties of novel sodium-ion battery materials.

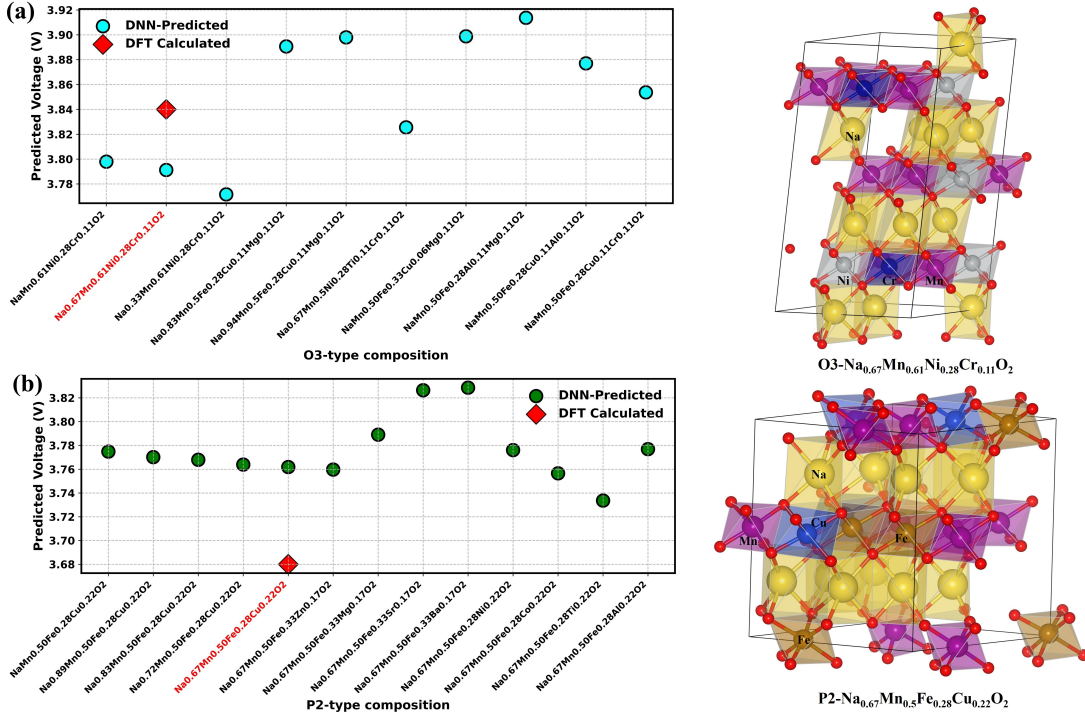


Figure 6: DNN predicted and DFT voltage of some specific cathode compositions for Na-ion batteries (a) O3-type and (b) P2-type.

Conclusions

This study demonstrates the power of combining machine learning (ML) with first-principles simulations to accelerate the discovery and optimization of next-generation Na-ion battery cathodes. Our deep neural network (DNN) model, trained on Density Functional Theory (DFT) data, achieves a mean absolute error (MAE) of 0.24V, outperforming existing voltage prediction models with a high level of accuracy and a deviation of less than 5%. To validate the predictive capability of our model, we compared its voltage estimations with DFT-calculated values for two newly investigated cathode compositions: O3-Na_{0.67}Mn_{0.61}Fe_{0.28}Cr_{0.11}O₂ and P2-Na_{0.67}Mn_{0.5}Fe_{0.28}Cu_{0.22}O₂. The excellent agreement between ML-predicted and DFT-computed voltages confirms the reliability of our approach in capturing the electrochemical behavior of Na-ion materials. By significantly reducing reliance on time-consuming and resource-intensive experimental methods, our approach provides a systematic framework for identifying promising cathode materials with optimized

electrochemical properties. This data-driven methodology enables rapid screening of novel compositions, guiding experimental efforts toward the most promising candidates.

The insights gained from this study contribute to the development of high-performance Na-ion batteries, offering a viable and sustainable alternative to Li-ion technology for future energy storage applications. By leveraging machine learning-driven material discovery, this work paves the way for the rational design of next-generation battery materials, supporting advancements in clean energy technologies and grid-scale storage solutions.

Acknowledgment

This work was supported by the Korea Institute of Science and Technology (Grant number 2E31851), GKP (Global Knowledge Platform, Grant number 2V6760) project of the Ministry of Science, ICT and Future Planning.

Conflicts of interest

The authors declare no conflict of interest.

Supporting Information Available

The supporting information file includes the definition of R^2 term, list of elemental features used for the building of the DNN model, computational methodology and expressions used for calculation of formation energy and voltage of new compositions. It also contains the structural information of two specific compositions, O3 and P2-type ordering (Figure S1). Formation energy of all the new compositions of O3 and P2-type ordering are presented in Figure S2.

References

- (1) Andersen, C. W.; Armiento, R.; Blokhin, E.; Conduit, G. J.; Dwaraknath, S.; Evans, M. L.; Fekete, Á.; Gopakumar, A.; Gražulis, S.; Merkys, A.; others OPTIMADE, an API for exchanging materials data. *Scientific data* **2021**, *8*, 217.
- (2) Evans, M. L.; Bergsma, J.; Merkys, A.; Andersen, C. W.; Andersson, O. B.; Beltrán, D.; Blokhin, E.; Boland, T. M.; Balderas, R. C.; Choudhary, K.; others Developments and applications of the OPTIMADE API for materials discovery, design, and data exchange. *Digital Discovery* **2024**, *3*, 1509–1533.
- (3) Evans, M. L.; Andersen, C. W.; Dwaraknath, S.; Scheidgen, M.; Fekete, Á.; Winston, D. optimade-python-tools: a Python library for serving and consuming materials data via OPTIMADE APIs. *The Journal of Open Source Software* **2021**, *6*.
- (4) Gashmard, H.; Shakeripour, H.; Alaei, M. Predicting superconducting transition temperature through advanced machine learning and innovative feature engineering. *Scientific Reports* **2024**, *14*, 3965.
- (5) Seegmiller, C. C.; Baird, S. G.; Sayeed, H. M.; Sparks, T. D. Discovering chemically novel, high-temperature superconductors. *Computational Materials Science* **2023**, *228*, 112358.
- (6) Yazdani-Asrami, M. Artificial intelligence, machine learning, deep learning, and big data techniques for the advancements of superconducting technology: a road to smarter and intelligent superconductivity. *Superconductor Science and Technology* **2023**, *36*, 084001.
- (7) Hui, Z.; Wang, M.; Yin, X.; Yue, Y.; others Machine learning for perovskite solar cell design. *Computational Materials Science* **2023**, *226*, 112215.

- (8) Bansal, N. K.; Mishra, S.; Dixit, H.; Porwal, S.; Singh, P.; Singh, T. Machine learning in perovskite solar cells: recent developments and future perspectives. *Energy Technology* **2023**, *11*, 2300735.
- (9) Bhatti, S.; Manzoor, H. U.; Michel, B.; Bonilla, R. S.; Abrams, R.; Zoha, A.; Hussain, S.; Ghannam, R. Revolutionizing low-cost solar cells with machine learning: a systematic review of optimization techniques. *Advanced Energy and Sustainability Research* **2023**, *4*, 2300004.
- (10) Valsalakumar, S.; Bhandari, S.; Roy, A.; Mallick, T. K.; Hinshelwood, J.; Sundaram, S. Machine learning driven performance for hole transport layer free carbon-based perovskite solar cells. *npj Computational Materials* **2024**, *10*, 212.
- (11) Ren, Z.; Li, H.; Yan, W.; Lv, W.; Zhang, G.; Lv, L.; Sun, L.; Sun, Z.; Gao, W. Comprehensive evaluation on production and recycling of lithium-ion batteries: A critical review. *Renewable and Sustainable Energy Reviews* **2023**, *185*, 113585.
- (12) Hatzell, K. B. Anode-less or anode-free? 2023.
- (13) Godbole, R.; Hiwase, S.; Hossain, M.; Kadam, S.; Wable, M.; Rane, S.; Mondal, S.; Das, B.; Banerjee, A.; Ogale, S. Light element (B, N) co-doped graphitic films on copper as highly robust current collectors for anode-free Li metal battery applications. *Applied Physics Reviews* **2024**, *11*.
- (14) Hu, J.; Hong, Y.; Guo, M.; Hu, Y.; Tang, W.; Xu, S.; Jia, S.; Wei, B.; Liu, S.; Fan, C.; others Emerging organic electrodes for Na-ion and K-ion batteries. *Energy Storage Materials* **2023**, *56*, 267–299.
- (15) Thirupathi, R.; Kumari, V.; Chakrabarty, S.; Omar, S. Recent progress and prospects of NASICON framework electrodes for Na-ion batteries. *Progress in Materials Science* **2023**, *137*, 101128.

- (16) Zhao, Y.; Liu, Q.; Zhao, X.; Mu, D.; Tan, G.; Li, L.; Chen, R.; Wu, F. Structure evolution of layered transition metal oxide cathode materials for Na-ion batteries: Issues, mechanism and strategies. *Materials Today* **2023**, *62*, 271–295.
- (17) Nie, C.; Wang, G.; Wang, D.; Wang, M.; Gao, X.; Bai, Z.; Wang, N.; Yang, J.; Xing, Z.; Dou, S. Recent Progress on Zn Anodes for Advanced Aqueous Zinc-Ion Batteries. *Advanced Energy Materials* **2023**, *13*, 2300606.
- (18) Pandey, D. K.; Hunjra, A. I.; Bhaskar, R.; Al-Faryan, M. A. S. Artificial intelligence, machine learning and big data in natural resources management: a comprehensive bibliometric review of literature spanning 1975–2022. *Resources Policy* **2023**, *86*, 104250.
- (19) Sarker, I. H. Machine learning: Algorithms, real-world applications and research directions. *SN computer science* **2021**, *2*, 160.
- (20) Jain, A.; Ong, S. P.; Hautier, G.; Chen, W.; Richards, W. D.; Dacek, S.; Cholia, S.; Gunter, D.; Skinner, D.; Ceder, G.; others Commentary: The Materials Project: A materials genome approach to accelerating materials innovation. *APL materials* **2013**, *1*.
- (21) Kirklin, S.; Saal, J. E.; Meredig, B.; Thompson, A.; Doak, J. W.; Aykol, M.; Rühl, S.; Wolverton, C. The Open Quantum Materials Database (OQMD): assessing the accuracy of DFT formation energies. *npj Computational Materials* **2015**, *1*, 1–15.
- (22) Saal, J. E.; Kirklin, S.; Aykol, M.; Meredig, B.; Wolverton, C. Materials design and discovery with high-throughput density functional theory: the open quantum materials database (OQMD). *Jom* **2013**, *65*, 1501–1509.
- (23) Curtarolo, S.; Setyawan, W.; Wang, S.; Xue, J.; Yang, K.; Taylor, R. H.; Nelson, L. J.; Hart, G. L.; Sanvito, S.; Buongiorno-Nardelli, M.; others AFLOWLIB.ORG: A distributed materials properties repository from high-throughput ab initio calculations. *Computational Materials Science* **2012**, *58*, 227–235.

- (24) Ortiz, C.; Eriksson, O.; Klintonberg, M. Data mining and accelerated electronic structure theory as a tool in the search for new functional materials. *Computational Materials Science* **2009**, *44*, 1042–1049.
- (25) Landis, D. D.; Hummelshøj, J. S.; Nestorov, S.; Greeley, J.; Duřak, M.; Bligaard, T.; Nørskov, J. K.; Jacobsen, K. W. The computational materials repository. *Computing in Science & Engineering* **2012**, *14*, 51–57.
- (26) Draxl, C.; Scheffler, M. NOMAD: The FAIR concept for big data-driven materials science. *Mrs Bulletin* **2018**, *43*, 676–682.
- (27) Bergerhoff, G.; Hundt, R.; Sievers, R.; Brown, I. The inorganic crystal structure data base. *Journal of chemical information and computer sciences* **1983**, *23*, 66–69.
- (28) Gražulis, S.; Daškevič, A.; Merkys, A.; Chateigner, D.; Lutterotti, L.; Quiros, M.; Serebryanaya, N. R.; Moeck, P.; Downs, R. T.; Le Bail, A. Crystallography Open Database (COD): an open-access collection of crystal structures and platform for worldwide collaboration. *Nucleic acids research* **2012**, *40*, D420–D427.
- (29) Bole, B.; Kulkarni, C. S.; Daigle, M. Adaptation of an electrochemistry-based li-ion battery model to account for deterioration observed under randomized use. Annual conference of the PHM society. 2014.
- (30) Hogge, E. F.; Bole, B. M.; Vazquez, S. L.; Celaya, J. R.; Strom, T. H.; Hill, B. L.; Smalling, K. M.; Quach, C. C. Verification of a remaining flying time prediction system for small electric aircraft. Annual conference of the phm society. 2015.
- (31) Joshi, R. P.; Eickholt, J.; Li, L.; Fornari, M.; Barone, V.; Peralta, J. E. Machine learning the voltage of electrode materials in metal-ion batteries. *ACS applied materials & interfaces* **2019**, *11*, 18494–18503.

- (32) Moses, I. A.; Joshi, R. P.; Ozdemir, B.; Kumar, N.; Eickholt, J.; Barone, V. Machine learning screening of metal-ion battery electrode materials. *ACS Applied Materials & Interfaces* **2021**, *13*, 53355–53362.
- (33) Louis, S.-Y.; Siriwardane, E. M. D.; Joshi, R. P.; Omeo, S. S.; Kumar, N.; Hu, J. Accurate prediction of voltage of battery electrode materials using attention-based graph neural networks. *ACS Applied Materials & Interfaces* **2022**, *14*, 26587–26594.
- (34) Sendek, A. D.; Yang, Q.; Cubuk, E. D.; Duerloo, K.-A. N.; Cui, Y.; Reed, E. J. Holistic computational structure screening of more than 12000 candidates for solid lithium-ion conductor materials. *Energy & Environmental Science* **2017**, *10*, 306–320.
- (35) Li, J.; Zhou, M.; Wu, H.-H.; Wang, L.; Zhang, J.; Wu, N.; Pan, K.; Liu, G.; Zhang, Y.; Han, J.; others Machine Learning-Assisted Property Prediction of Solid-State Electrolyte. *Advanced Energy Materials* **2024**, 2304480.
- (36) Mishra, A. K.; Rajput, S.; Karamta, M.; Mukhopadhyay, I. Exploring the possibility of machine learning for predicting ionic conductivity of solid-state electrolytes. *ACS omega* **2023**, *8*, 16419–16427.
- (37) Hu, S.; Huang, C. Machine-learning approaches for the discovery of electrolyte materials for solid-state lithium batteries. *Batteries* **2023**, *9*, 228.
- (38) Ferraz-Caetano, J.; Teixeira, F.; Cordeiro, M. N. D. Explainable supervised machine learning model to predict solvation gibbs energy. *Journal of Chemical Information and Modeling* **2023**, *64*, 2250–2262.
- (39) Alibakhshi, A.; Hartke, B. Improved prediction of solvation free energies by machine-learning polarizable continuum solvation model. *Nature Communications* **2021**, *12*, 3584.

- (40) Ward, L.; Dandu, N.; Blaiszik, B.; Narayanan, B.; Assary, R. S.; Redfern, P. C.; Foster, I.; Curtiss, L. A. Graph-based approaches for predicting solvation energy in multiple solvents: open datasets and machine learning models. *The Journal of Physical Chemistry A* **2021**, *125*, 5990–5998.
- (41) Manna, S. S.; Manna, S.; Pathak, B. Molecular dynamics-machine learning approaches for the accurate prediction of electrochemical windows of ionic liquid electrolytes for dual-ion batteries. *Journal of Materials Chemistry A* **2023**, *11*, 21702–21712.
- (42) Zhang, Y.; Shi, C.; Brennecke, J. F.; Maginn, E. J. Refined method for predicting electrochemical windows of ionic liquids and experimental validation studies. *The Journal of Physical Chemistry B* **2014**, *118*, 6250–6255.
- (43) Baskin, I.; Epshtein, A.; Ein-Eli, Y. Benchmarking machine learning methods for modeling physical properties of ionic liquids. *Journal of Molecular Liquids* **2022**, *351*, 118616.
- (44) Thelen, A.; Huan, X.; Paulson, N.; Onori, S.; Hu, Z.; Hu, C. Probabilistic machine learning for battery health diagnostics and prognostics—review and perspectives. *npj Materials Sustainability* **2024**, *2*, 14.
- (45) Zou, J.; Gao, Y.; Frieges, M. H.; Börner, M. F.; Kampker, A.; Li, W. Machine learning for battery quality classification and lifetime prediction using formation data. *Energy and AI* **2024**, *18*, 100451.
- (46) Sekhar, J. C.; Domathoti, B.; Santibanez Gonzalez, E. D. Prediction of battery remaining useful life using machine learning algorithms. *Sustainability* **2023**, *15*, 15283.
- (47) Ling, C. A review of the recent progress in battery informatics. *npj Computational Materials* **2022**, *8*, 33.
- (48) Ong, S. P.; Cholia, S.; Jain, A.; Brafman, M.; Gunter, D.; Ceder, G.; Persson, K. A. The Materials Application Programming Interface (API): A simple, flexible and efficient

- API for materials data based on REpresentational State Transfer (REST) principles. *Computational Materials Science* **2015**, *97*, 209–215.
- (49) Ward, L.; Dunn, A.; Faghaninia, A.; Zimmermann, N. E.; Bajaj, S.; Wang, Q.; Montoya, J.; Chen, J.; Bystrom, K.; Dylla, M.; others Matminer: An open source toolkit for materials data mining. *Computational Materials Science* **2018**, *152*, 60–69.
- (50) Liu, C.; Fujita, E.; Katsura, Y.; Inada, Y.; Ishikawa, A.; Tamura, R.; Kimura, K.; Yoshida, R. Machine learning to predict quasicrystals from chemical compositions. *Advanced Materials* **2021**, *33*, 2102507.
- (51) Pham, T. L.; Kino, H.; Terakura, K.; Miyake, T.; Tsuda, K.; Takigawa, I.; Dam, H. C. Machine learning reveals orbital interaction in materials. *Science and technology of advanced materials* **2017**, *18*, 756.
- (52) Paszke, A.; Gross, S.; Chintala, S.; Chanan, G.; Yang, E.; DeVito, Z.; Lin, Z.; Desmaison, A.; Antiga, L.; Lerer, A. Automatic differentiation in PyTorch. NIPS-W. 2017.
- (53) Paszke, A.; Gross, S.; Massa, F.; Lerer, A.; Bradbury, J.; Chanan, G.; Killeen, T.; Lin, Z.; Gimelshein, N.; Antiga, L.; others Pytorch: An imperative style, high-performance deep learning library. *Advances in neural information processing systems* **2019**, *32*.
- (54) Kingma, D. P. Adam: A method for stochastic optimization. *arXiv preprint arXiv:1412.6980* **2014**,
- (55) Amatucci, G.; Tarascon, J.; Klein, L. CoO₂, the end member of the Li x CoO₂ solid solution. *Journal of The Electrochemical Society* **1996**, *143*, 1114.
- (56) Delmas, C.; Ménétrier, M.; Croguennec, L.; Levasseur, S.; Pérès, J.; Poullierie, C.; Prado, G.; Fournes, L.; Weill, F. Lithium batteries: a new tool in solid state chemistry. *International Journal of Inorganic Materials* **1999**, *1*, 11–19.

- (57) Li, G.; Azuma, H.; Tohda, M. LiMnPO₄ as the cathode for lithium batteries. *Electrochemical and Solid-State Letters* **2002**, *5*, A135.
- (58) Amine, K.; Yasuda, H.; Yamachi, M. Olivine LiCoPO₄ as 4.8 V electrode material for lithium batteries. *Electrochemical and Solid-State Letters* **2000**, *3*, 178.
- (59) Priyono, S.; Hardiyani, S.; Syarif, N.; Subhan, A.; Suhandi, A. Electrochemical performance of LiMn₂O₄ with varying thickness of cathode sheet. *Journal of Physics: Conference Series*. 2019; p 012022.
- (60) Whittingham, M. S. Electrical energy storage and intercalation chemistry. *Science* **1976**, *192*, 1126–1127.
- (61) Wolfenstine, J.; Allen, J. Ni³⁺/Ni²⁺ redox potential in LiNiPO₄. *Journal of Power Sources* **2005**, *142*, 389–390.
- (62) Gaubicher, J.; Wurm, C.; Goward, G.; Masquelier, C.; Nazar, L. Rhombohedral form of Li₃V₂(PO₄)₃ as a cathode in Li-ion batteries. *Chemistry of materials* **2000**, *12*, 3240–3242.
- (63) Delmas, C.; Braconnier, J.-J.; Fouassier, C.; Hagemmuller, P. Electrochemical intercalation of sodium in Na_xCoO₂ bronzes. *Solid State Ionics* **1981**, *3*, 165–169.
- (64) Berthelot, R.; Carlier, D.; Delmas, C. Electrochemical investigation of the P₂-Na_xCoO₂ phase diagram. *Nature materials* **2011**, *10*, 74–80.
- (65) Braconnier, J.; Delmas, C.; Hagemmuller, P. Etude par desintercalation electrochimique des systemes Na_xCrO₂ et Na_xNiO₂. *Materials Research Bulletin* **1982**, *17*, 993–1000.
- (66) Maazaz, A.; Delmas, C.; Hagemmuller, P. A study of the Na_xTiO₂ system by electrochemical deintercalation. *Journal of inclusion phenomena* **1983**, *1*, 45–51.
- (67) Moreau, P.; Guyomard, D.; Gaubicher, J.; Boucher, F. Structure and stability of sodium intercalated phases in olivine FePO₄. *Chemistry of Materials* **2010**, *22*, 4126–4128.

- (68) Tarascon, J.-M. Na-ion versus Li-ion batteries: complementarity rather than competitiveness. *Joule* **2020**, *4*, 1616–1620.
- (69) Abraham, K. How comparable are sodium-ion batteries to lithium-ion counterparts? *ACS Energy Letters* **2020**, *5*, 3544–3547.
- (70) Chayambuka, K.; Mulder, G.; Danilov, D. L.; Notten, P. H. From li-ion batteries toward Na-ion chemistries: challenges and opportunities. *Advanced energy materials* **2020**, *10*, 2001310.
- (71) Sayahpour, B.; Hirsh, H.; Parab, S.; Nguyen, L. H. B.; Zhang, M.; Meng, Y. S. Perspective: Design of cathode materials for sustainable sodium-ion batteries. *MRS Energy & Sustainability* **2022**, *9*, 183–197.
- (72) Okhotnikov, K.; Charpentier, T.; Cadars, S. Supercell program: a combinatorial structure-generation approach for the local-level modeling of atomic substitutions and partial occupancies in crystals. *Journal of cheminformatics* **2016**, *8*, 1–15.
- (73) Kresse, G.; Joubert, D. From ultrasoft pseudopotentials to the projector augmented-wave method. *Physical review b* **1999**, *59*, 1758.
- (74) Kresse, G.; Furthmüller, J. Efficient iterative schemes for ab initio total-energy calculations using a plane-wave basis set. *Physical review B* **1996**, *54*, 11169.
- (75) Perdew, J. P.; Burke, K.; Ernzerhof, M. Generalized gradient approximation made simple. *Physical review letters* **1996**, *77*, 3865.
- (76) Grimme, S.; Antony, J.; Ehrlich, S.; Krieg, H. A consistent and accurate ab initio parametrization of density functional dispersion correction (DFT-D) for the 94 elements H-Pu. *The Journal of chemical physics* **2010**, *132*.
- (77) Wang, L.; Maxisch, T.; Ceder, G. Oxidation energies of transition metal oxides within

- the GGA+ U framework. *Physical Review B—Condensed Matter and Materials Physics* **2006**, *73*, 195107.
- (78) Wei, J.; Shaw, L.; Chen, W. First-principles prediction of Na diffusivity in doped NaCrO₂ layered cathode materials with van der Waals interactions. *The Journal of Physical Chemistry C* **2020**, *124*, 12239–12248.
- (79) Emery, A. A.; Wolverton, C. High-throughput DFT calculations of formation energy, stability and oxygen vacancy formation energy of ABO₃ perovskites. *Scientific data* **2017**, *4*, 1–10.
- (80) Mishra, N.; Boral, R.; Paul, T. Designing layered oxides as cathodes for sodium-ion batteries: Machine learning and density functional theory based modeling. *Materials Today Physics* **2025**, *51*, 101634.
- (81) Gwon, H.; Seo, D.-H.; Kim, S.-W.; Kim, J.; Kang, K. Combined first-principle calculations and experimental study on multi-component olivine cathode for lithium rechargeable batteries. *Advanced Functional Materials* **2009**, *19*, 3285–3292.

TOC Graphic

